A Holistic Analysis and Experimental Testing of a Passive Heat Path for Electric Motors Slots

Ahmed Hebala, Peter H. Connor, Stefano Nuzzo, Chris Gerada, Michael Galea

[1]***Abstract*- This paper presents a thorough and broad analysis of the passive slot heat path concept. Six heat path shapes are proposed and compared in terms of their combined thermal and electrical performance. Through an extensive search pool that covers a wide range of motor and slot designs and operating conditions, this paper assesses the heat removal capabilities of the heat path from the slot. The analysis is performed through a lumped parameter thermal network approach. Additionally, statistical analyses using correlations and linear regression models are carried out to improve understanding of this concept. Furthermore, a neural-network model is created to improve the regression model accuracy in predicting the slot temperature and temperature reduction. Finally, experimental testing and validation of the modelling are carried out on one of the six heat path shapes.**

Keywords- **Advanced Thermal Cooling Systems, Electrical Machine Design, Finite Element Analysis, Heat Path, Thermal Management, Lumped Parameter Thermal Network, Linear Regression, Neural Network Regression, Permanent Magnet Synchronous Motor.**

I. INTRODUCTION

The electrical machine is a key component in hybrid and electric powertrains of vehicles. Improving its design requires extensive research to achieve important performance metrics such as high efficiency, high power-density, and low cost to make a strong business case and expand the market [1]. While material advancements offer enhanced performance, new materials frequently come with a higher price. Improvements in thermal management have been proven to be crucial enablers for pushing technological boundaries [1]. This paper seeks to evaluate the performance of stator slot thermal heat paths (HPs) using affordable materials in multiple feasible shapes for their thermal characterisation and impact on machine performance.

Heat is generated in an electric motor during operation due to the various loss mechanisms within it. This heat can be dissipated through conduction, convection, and radiation to the surroundings. The losses must be quantified and mapped, and then a thermal model of the motor has to be developed to analyse the performance under different conditions [2], [3].

There are three main methods for thermal modelling used by engineers today. These are the Lumped Parameter Thermal Network (LPTN), thermal Finite Element Method (FEM) and Computational Fluid Dynamics (CFD) [4]. Considering the three methods, a trade-off between accuracy, ease of use and calculation time takes place to select which method to use. In an industry-based design process, LPTN is usually preferred for faster and more interactive design procedures. Additionally, it can be easily linked to electromagnetic design for a combined design optimisation process [4]-[7].

Regarding thermal management of electrical machines, there are several approaches for the installation of fins and ducts into the housing design to increase the motor's outer surface area to boost convective and radiative heat transfer. These have commonly been used to improve the natural cooling of electrical machines [8], [9]. Forced air cooling technologies generally provide improved thermal performance at the expense of increased complexity and additional components. The use of liquids enables high-performance cooling in either direct or indirect approaches. Liquid cooling is often favoured where a cooling circuit is already present within the wider system [10]. A stator jacket is a conventional and convenient means to provide liquid cooling. There are various ways to design stator water jackets [11]. Direct cooling solutions, such as oil-spray or directly cooled conductors, have been also widely used. The latter, however, is traditionally justified in large machines [12],[13].

Currently, active liquid cooling is adopted in high-performance machines such as in [14], [15] as well as flooded or semi-flooded cooling approaches [16], [17]. However, these techniques require significant sealing, which can lead to reliability issues, and they require parasitic pumping power, contrary to passive cooling approaches such as in-slot HPs. This paper is dedicated to investigating the concept of passive conductive in-slot HPs, which can work with motors regardless of the outer housing cooling method selected, thus eliminating risks, complications and costs associated with liquid in-slot cooling.

As the major loss source is usually the winding, it is necessary to enhance the thermal connection between the winding area and the coolant. Bringing the coolant flow closer to the windings to shorten the thermal path is very effective [18].

There has been a growing interest in passive methods for cooling electrical machines [19]-[23]. Heat guides/vanes/paths are one of the promising methods for transporting heat from the slot to the back iron to move the heat generation nearer to the convective coolant sink. This paper will explore the limits of the passive HP concept and how it can be utilised to improve the thermal performance of electrical machines.

[1] This work is funded by the INNOVATIVE doctoral programme. The INNOVATIVE programme is partially funded by the Marie Curie Initial Training Networks (ITN) action (project number 665468) and partially by the Institute for Aerospace Technology (IAT) at the University of Nottingham, UK.

Ahmed Hebala is with the Electrical and Control Engineering department, Arab Academy for Science, Technology and Maritime Transport, Alexandria, Egypt; ahmed.hebala@aast.edu

Ahmed Hebala, Peter H. Connor and Chris Gerada are with the Power Electronics, Machines and Control (PEMC) Research Group, Faculty of Engineering, University of Nottingham, Nottingham, UK; ahmed.hebala@nottingham.ac.uk, peter.connor@nottingham.ac.uk, chris.gerada@nottingham.ac.uk.

Stefano Nuzzo is with the Department of Engineering Enzo Ferrari, University of Modena and Reggio Emilia, Modena, Italy; stefano.nuzzo@unimore.it

Michael Galea is with the Department of Electrical Engineering, University of Malta, MSD 2080 Msida, Malta; michael.d.galea@um.edu.mt.

In [22] axial and annular HPs were introduced. A trade-off between the heat transfer rate, copper losses, the number and size of the axial ducts or an additional annular gap between the winding and the machine air gap was made. Using the annular gap or axial duct designs with water cooling, winding hotspot temperatures can be reduced by more than 40 °C. However, these methods were applied to smaller motors operating at high speeds, were for a slot-less design [22], and required sealing and generated fluid pumping losses.

In [22], several methods were proposed for convective and conductive heat removal. This included the use of graphite sheets that have thicknesses of roughly 100 micrometres and thermal conductivities of around 700 W/m·K in the form of sheets of suitable materials inserted into the winding pack. Yet, when compared to jacket cooling, this methodology provides no additional benefit [22].

This paper aims to enhance the performance of dry-passive HPs by studying and understanding the effects of different HP shapes. The main contribution of this paper lies in its holistic analysis, which adds multiple layers of deep and broad examination to the concept of passive in-slot HPs.

Firstly, six HP shapes are proposed, covering a broader range of options than previously available in the literature, as discussed in Section II. Secondly, the comprehensive analysis captures and simulates various parameters, including machine dimensions, slot shapes, cooling conditions, heat path sizes, and anisotropic behaviour. This extensive study explores a wide range of designs and possibilities, furthering the understanding and scope of the HP concept, which is also elaborated in Section II.

Thirdly, while the LPTN has been widely used, the implementation here is generic. The proposed network models normal operation without a HP and all six shapes for any machine design and operating condition within the paper's scope. Typically, LPTN lacks adaptability, but the proposed LPTN can fit all these variations in an agile manner, as described in Section II.

Fourthly, a motor design paradigm is introduced, including a helpful algorithm for scanning a wide pool of machine designs, especially during the initial design stages, as outlined in Section III.

A fifth aspect of the contribution is the data analysis, which provides insights into the main factors contributing to the success of the HP through correlation analysis and other methods, as presented in Section IV. Both linear and neural network (NN) regression models are intended to facilitate the implementation and adoption of the HP by other researchers. These models also serve as a method for estimating the HP performance for any given operating condition or machine design, providing a good first guess and accelerating the design process, as detailed in Section IV.

The proposed models are verified through experimental testing of the proposed HP in Section V. Additionally, losses are modelled and evaluated for the HP in Section VI to assess the realistic benefits of the proposed concept against its possible drawbacks. Finally, conclusions are drawn in Section VII.

II. PROPOSED SHAPES AND SEARCH SPACE

Six different HP shapes are proposed for this analysis, as shown in Fig. 1. The models and calculations are based on an angular single-slot sector of a stator, shown as a rectangular shape for simplicity. This analysis is based on a conventional inner rotor design, thus providing a benchmark study and guiding the design of HPs for radial flux, inner rotor motors.

a. Proposed Shapes

The baseline design is indicated as design 'O', where no HP is used as shown in Fig. 1(g). For the purposes of aiding the reader, symbols representing the basic shapes of the heat paths are inserted into the text. The HP shapes are also designated with the following simple text symbols within this paper as a reminder to the reader of their design such as A is |, B is ⊥, C is ||, D is |||, E is ⊤, and F is ┼.

Each of the HP concepts has been devised to study the individual effects caused by radial and tangential positioning of the HP materials, thickness and position of the paths and combinations of these factors. When coupled with materials of isotropic or anisotropic thermal conductivity values, these shapes have a variety of performance influences on the cooling.

Shapes 'A', 'C' and D' comprise straight HPs only in the radial direction. Shapes 'B', 'E' and 'F' combine tangential direction components in combination with radial HPs.

Shapes C '||' and D '|||', as shown in Fig. 1(c) and Fig. 1(d) respectively, are variations of design A. They subdivide the same HP cross-sectional width into two and three radial paths of equal thickness and separation, respectively. In each case, the thickness of the tangential parts in B, E and F is half the thickness of the radial parts of the HP. Manufacturing and assembly complexities for winding around the various HP shapes should also be taken into account.

b. The proposed LPTN Model

A LPTN model is proposed to analyse the HP effectiveness. This proposed LPTN model is validated using experimental testing (see section VI). The slot centre and tooth centre present symmetry conditions, thus adiabatic boundary conditions are imposed to emulate the symmetry condition caused by neighbouring slots.

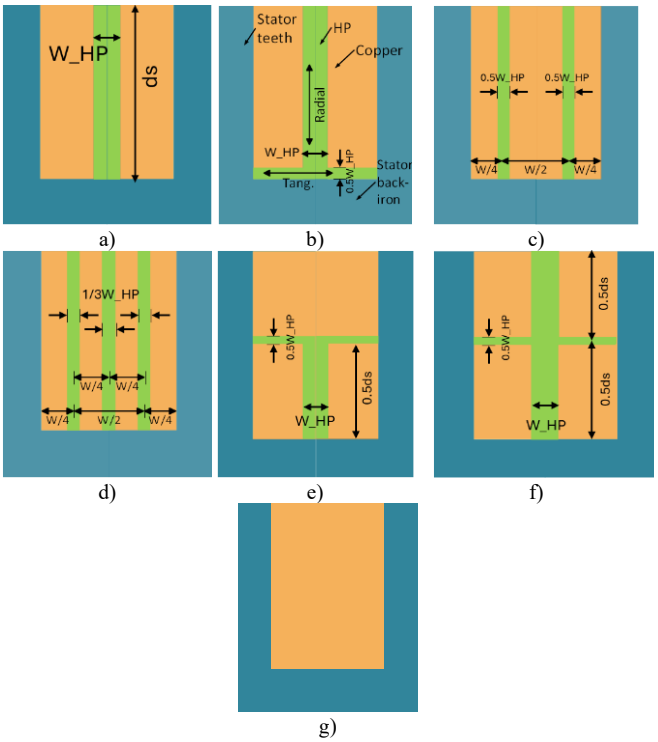

Fig. 1: Proposed HP shapes, a) shape A, b) shape B, c) shape C, d) Shape D, e) shape E, f) shape f, g) No HP.

The resistance matrix shown in Fig. 2 is calculated from both the conduction and convection conditions, as dictated by (1)-(5), whereas radiation effects are assumed to be negligible through the airgap and stator outer surface so are not modelled. Ideal contact is assumed between the HP and neighbouring materials for this study. Only thermal steady-state is considered with constant temperatures for the ambient air and cooling liquid of 40 °C.

A classical approach would be creating a different LPTN model for each of the 6 HP shapes, plus another model for the slot with no HP. This paper develops a more efficient, flexible, and novel way to model the HP shapes, as shown in Fig. 3. The proposed modelling approach employs the similarities between the HP shapes, by creating a generic LPTN 2D model which includes an overlay of all the HPs designs, as illustrated in Fig. 3. The model is modified to change each slot zone accordingly to represent the winding and HP material layout, conductivity, and loss distribution.

The distribution of the nodes and their locations is depicted in Fig. 2. A total of 55 nodes are selected, as shown in the LPTN model. Only half of the slot is modelled, utilising the symmetry boundary condition, while maintaining accuracy and reducing modelling and analysis time. The resistance network consists of connections in both the radial and tangential directions, and a convective heat transfer boundary condition on the airgap and stator outer surfaces is applied, as shown in Fig. 2.

c. LPTN Model Equations

The LPTN model uses the analogy between electrical and thermal model phenomena. In (1)-(3), the n-node network equations are listed, where P is the power loss vector, T is the temperature at each node, and G is the thermal admittance matrix.

$$[P]_{n\times 1} = [G]_{n\times n}\ [T]_{n\times 1} \tag{1}$$

$$[T]_{n\times 1} = [G]^{-1}_{n\times n}\ [P]_{n\times 1} \tag{2}$$

$$G = \begin{bmatrix} \sum_{i=1}^{n}\frac{1}{R_{1,i}} & \frac{-1}{R_{1,2}} & \cdots & \frac{-1}{R_{1,n}} \\ \frac{-1}{R_{2,1}} & \sum_{i=2}^{n}\frac{1}{R_{2,i}} & \cdots & \frac{-1}{R_{2,n}} \\ \vdots & \vdots & \ddots & \vdots \\ \frac{-1}{R_{n,1}} & \frac{-1}{R_{n,2}} & \cdots & \sum_{i=n}^{n}\frac{1}{R_{n,i}} \end{bmatrix} \tag{3}$$

The conductive and convective thermal resistances are calculated based on (4) and (5), where l_{th} is the length through the thermal path, and A_{th} is the cross-section area of the thermal path.

$$R_{conduction\_th} = \frac{l_{th}}{A_{th} \times k} \tag{4}$$

$$R_{convection\_th} = \frac{1}{A_{th} \times htc} \tag{5}$$

III. MOTOR DESIGN METHODOLOGY

In this section, the adopted methodology of designing the motor is explored, further expanding on Table I. As stated earlier, 10 independent variables are used to generate the search space. Also, the main dimensions are shown in Fig. 4.

The contribution of the paper is to cover a wide range of motor sizes and operating conditions. Table I defines the number and nature of the variables which define the slot and motor shape. There are 10 independent variables and 8 dependent variables defined. Several factors are fixed, such as the slot fill factor, thermal conductivities of the core, winding and impregnation.

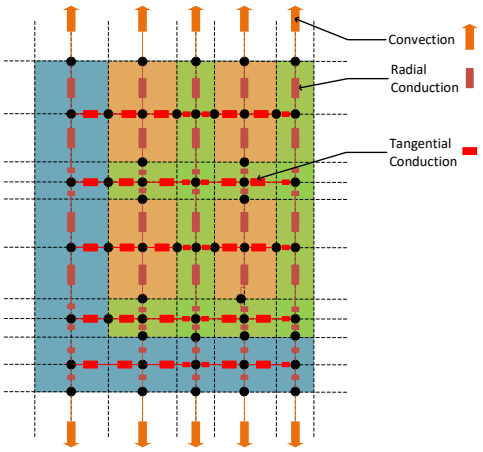

b)

Fig. 2: Proposed generic LTPN half-slot node locations.

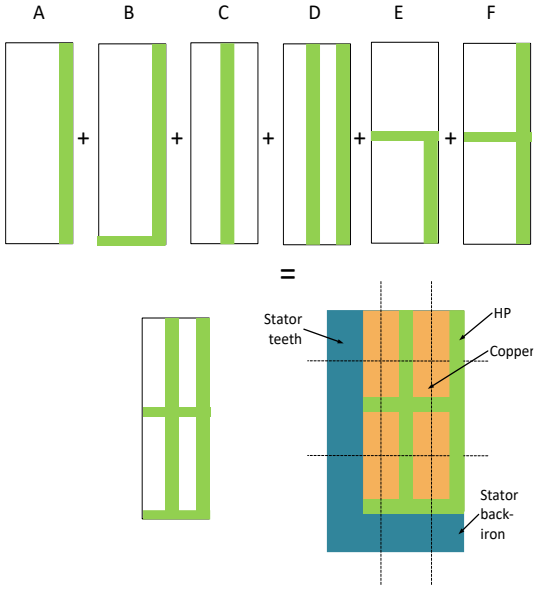

Fig. 3: Proposed generic half slot model based on overlay of the HP. shapes

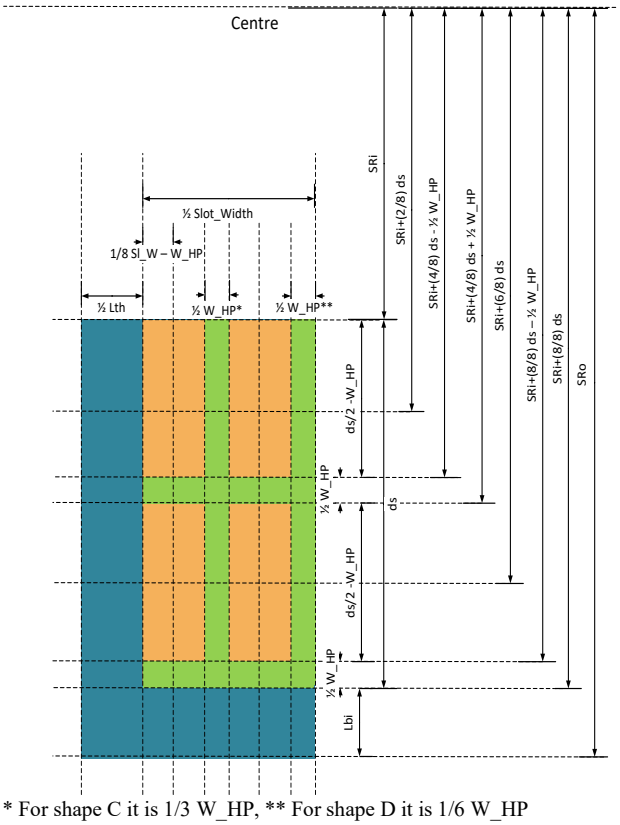

* For shape C it is 1/3 W_HP, ** For shape D it is 1/6 W_HP

Fig. 4: Slot dimensions and geometry.

The variables are broadly divided into geometrical and thermal categories. The wide ranges of geometrical motor and slot sizes considered represent a very wide range of potential motor frame sizes and output powers. The sizes were particularly suitable for aerospace applications, but the results are still valid for other machine applications.

The full factorial analysis for all of the variables would be expressed as $SS = m^x$, where SS is the search space size, m is the number of steps per variable, and x is the number of independent variables. Thus, the number of variations would exceed 9 million simulations for only five steps and equal to 10 billion for 10 steps. Thus, a search space reduction is proposed. In this case, Latin Hypercube Sampling (LHS) is adopted to reduce the required number of samples. LHS is a statistical method for generating a near-random sample of parameter values from a multidimensional distribution [24],[25]. Yet, extensive data post-processing and regression models are crucial. Hence, this is a major improvement and pragmatic approach.

The thermal conductivity of the HP is set to be anisotropic. In this case, the values of the radial and tangential HP thermal conductivity can vary independently. HPs are conventionally oriented so the major thermal conductivity would be in the radial direction. The maximum typically found in electrical machines is typically copper with a value of approximately 400 W/mK, so this is considered the maximum value used in this study. The minimum value for a convective boundary condition is selected to be 5 W/m^2K, which represents the minimum value likely found for natural convection cooling surfaces on a motor.

The losses are distributed based on the density of power loss in the winding area rather than absolute values.

The slot dimensions are shown in Fig. 4. Based on the first 4 parameters, the rest of the motor's stator dimensions are as follows:

$$SRo = SRi \,/\, ST\_AR \tag{6}$$

Then, the motor's stack length is defined by (9):

$$Lstk = SRo \times MT\_AR \tag{7}$$

The width of the slot opening is found through (10):

$$bs1 = (SRo - SRi) \,/\, SL\_AR \tag{8}$$

For all cases, it is assumed that the slot opening, the tooth width and the stator back iron thickness are equal. For simplicity, the slot is perceived as an open shape, i.e., there is no slot opening depth or height. While the assumptions do not consider the electromagnetic feasibility, they allow the changes for the thermal modelling to focus on the slot and HP behaviours and reduce the design space. Similarly, changing the back iron convection (resistance) is analogous to changing the back iron thickness so the search space is reduced by one variable, as the other effects may be inferred from the results. The slot width at the bottom of the slot, i.e., near the back iron is computed as (11), while the slot depth is processed as (12).

$$bs2 = \mathrm{bs1} \times (SRo - dc) \,/\, SRi \tag{9}$$

$$ds = SRo - SRi - dc \tag{10}$$

The number of slots is then calculated as (13):

$$Slots = \mathrm{round}\,(2\,\Pi\,SRi \,/\, (Tth + bs1)) \tag{11}$$

The fill factor, defined as the ratio between the conductors' area (including the wire insulation) and the slot area (excluding the liner), is fixed at 0.6 for the design with no HP. The slot impregnation thermal conductivity is 0.5 W/mK, and the stator core steel conductivity is 25 W/mK. Finally, the copper thermal conductivity is 385 W/mK.

TABLE I
MOTOR PARAMETERS AND DEPENDENCIES

Parameter (unit)	*Symbol*	*Range /Value*
HP shape	-	A:F
Stator inner radius (mm)	SRi	50.0: 500.0
Stator outer radius (mm)	SRo	(8)
Slot aspect ratio	SL_AR	1.0: 10.0
Stator aspect ratio	ST_AR	0.4:0.8
Motor aspect ratio	MT_AR	0.3:3
Stack length (mm)	Lstk	(9)
Slot width at slot opening (mm)	bs1	(10)
Slot width at slot bottom (mm)	bs2	(11)
Teeth width (mm)	Tth	= bs1
Stator back iron (mm)	dc	= Tth
Slot depth (mm)	ds	(12)
Slot average width (mm)	bs	f(bs1, bs2. ds)
HP Width (mm)	HP_Width	0.2:2.0
Fill Factor	FF	0.6
HP radial thermal conductivity (W/mK)	khp_R	5:400
HP circumferential conductivity (W/mK)	khp_C	5:400
Air gap thermal convection rate (W/m^2K)	htc_ag	5:200
Back iron thermal convection rate (W/m^2K)	htc_bi	500: 3000
Steel thermal conductivity (W/mK)	kst	25
Copper thermal conductivity (W/mK)	kcu	385
Slot impregnation thermal conductivity (W/mK)	kimp	0.5
Copper loss density (W/kg)	Pd_Cu	5:600
HP loss density (W/kg)	Pd_HP	0.5:60

Further calculations are made to define the thermal network resistance matrix based on the defined motor dimensions and the thermal aspects of the cooling and loss input parameters.

IV. RESULTS ANALYSIS

The section discusses the analysis results generated for this proposed study. These results represent a search space of over 18,000 design variations.

a. Overall Results Trends

As thousands of designs are evaluated, individual design analyses are very challenging. Therefore, an overall analysis of the results and a discussion of the general trends are incorporated. Later, a more detailed analysis of different variable relations and effects on the HP performance is performed.

It was noted that the temperatures of the non-HP designs noted as T_O, range from 50 °C to 250 °C. T_A is used to designate the peak (hotspot) temperature of copper for the shape A design and so forth for the other five HPs (B, C, D, E and F). The average of peak temperatures of T_o is 150.8 °C, and for the other six models with a HP, the averages of peak temperatures are 133.5 °C, 125.3 °C, 134.3 °C, 130.8 °C, 143.4 °C and 132.1 °C, respectively for shapes A to F. The overall trend suggests that the HP of shape B yields the lowest peak temperatures, whereas shape E has high average peaks.

An improved way of assessing the HP designs is based on the temperature difference i.e., the reduction criterion. The temperature difference here is defined as the difference between the peak temperature of the non-HP-based slot and the HP-based slots such as $Td_A = T_O - T_A$ and so on for the other five HP shapes. A histogram showing the probability of the temperature differences is depicted in Fig. 5, indicating how often each temperature difference value occurs within the dataset. The data show a temperature reduction of up to 100 °C. The average temperature reduction is 17.2 °C, 25.5

This article has been accepted for publication in IEEE Transactions on Transportation Electrification. This is the author's version which has not been fully edited and content may change prior to final publication. Citation information: DOI 10.1109/TTE.2025.3537161

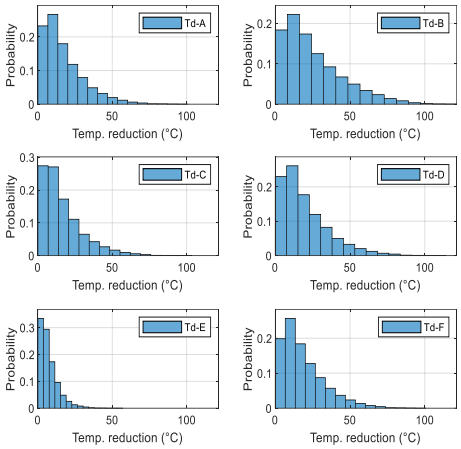

Fig. 5: Histogram of the temperature difference across the HP designs.

°C, 16.5 °C, 20.0 °C, 7.4 °C, 18.6 °C, for shapes A to F, respectively. Shape B with the inverted T prevailed as the most effective for temperature reduction, as it has the largest contact area with the slot's bottom, thus being closest to the liquid cooling medium. Shape D '|||' with the three radial parts and shape F '+' shaped as a cross come in second and third. Shape D benefits from the three radial HPs, thus spreading the heat but has a limited contact area with the slot bottom. Shape F utilises the tangential part of the HP to evenly distribute the heat flow from the centre to the sides and the bottom as well.

Despite their thermal benefits, both shapes D and F could be challenging for manufacturing and winding assembly.

In terms of ranking of the performance of each HP, the results show that in 88.4% of the designs, design B is the most effective in reducing temperatures.

Whereas the second-best design is D at 75.1% of being either the best or the second-best performing HP. HP of shape E is the lowest in terms of heat reductions, as there is no direct contact between the HP and airgap, and the contact between the HP and bottom of the slot is limited to a single point thus lower conductivity to the back iron cooling.

b. Specific Results Trends

Furthermore, the results are broken down into groups to draw more conclusions and trends. The results shown in Fig. 6 show the mean of the temperature differences based on the designs being divided into categories such as the width of the HP, the thermal conductivity across the HP thickness, and the

slot aspect ratio. The results in Fig. 6(a) show that the variation in temperature reductions, due to the slot aspect ratio, is limited for HP-shaped B, E and F. On the other hand, higher levels of slot aspect ratios, i.e., deeper slots, drive higher temperature reduction for shapes C and D.

The HP width also plays a strong role in increasing the HP effectiveness. As it can be noted in Fig. 6(b), almost a linearly spaced increase in the slot peak temperature reduction is experienced among all the HP designs with the HP width. Nevertheless, this increased width of the HP comes at the expense of less copper area and more complex assembly procedures.

Fig. 6(c) explores the variation of temperature reduction from the perspective of thermal conductivity in the radial direction of the HP. An increase in khp_R usually means higher grade material and more expensive purchase costs. A wide variation in temperature performance appears between those categorised at lower levels of conductivity from 5 to 100 W/mK when compared to the other three groups of

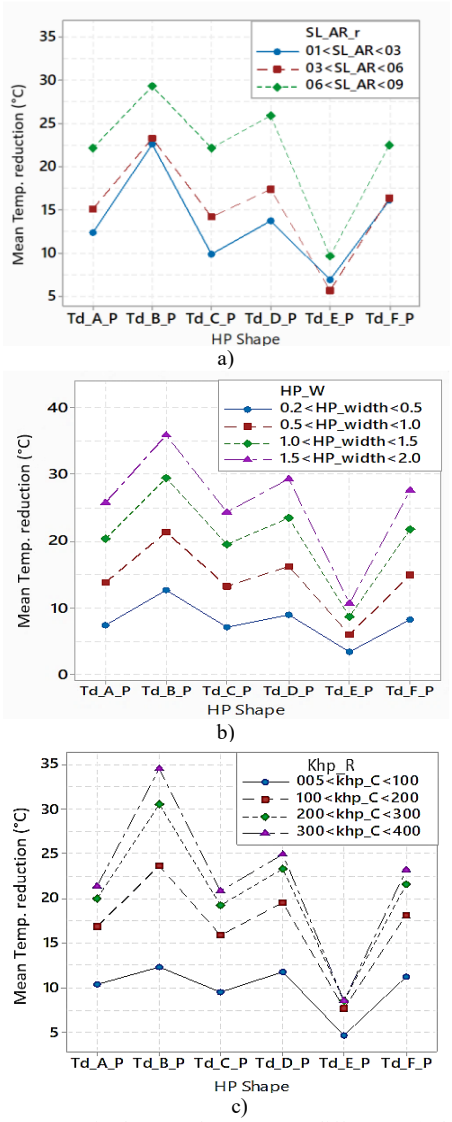

Fig. 6: Categorised mean of temperature difference, a) slot aspect ratio, b) HP width, c) HP radial thermal conductivity.

conductivity up to 400 W/mK. Thus, it can be advised to seek materials where the radial thermal conductivity is at least higher than 100 W/mK.

c. Correlation Analysis

This subsection seeks to determine which HP input parameters correlate to the most effective reductions in temperature.

The results are listed in Table II, showing the relationships between the input parameters and the peak slot temperature differences, as well as the peak temperature of the non-HP designs. The table is colour-mapped for ease of reading. The 10 independent variables defined earlier are considered here as well as four of the most common characteristics of electric motors, including the stack length, number of slots, slot depth and average width.

In Table II, T_O is negatively correlated to the number of slots and the stator aspect ratio, hence fewer number of slots and shorter slots tend to be cooler. For T_O, the relationship between HP width and thermal conductivities is blanked out since there is no HP in these slots. The correlation between T_O and the number of slots is weakly inverse, which conforms with the literature [26], where a higher number of slots usually coincides with lower copper temperature. This is caused by an effective increase in the slot-to-tooth contact area and a shortening of the conduction path between the slot

TABLE II
CORRELATION ANALYSIS

%	$Td_A = T_O - T_A$	$Td_B = T_O - T_B$	$Td_C = T_O - T_C$	$Td_D = T_O - T_D$	$Td_E = T_O - T_E$	$Td_F = T_O - T_F$
Slots	0.18	0.06	0.22	0.19	0.13	0.12
SID	0.12	0.15	0.12	0.13	0.10	0.13
Lstk	0.10	0.12	0.10	0.10	0.08	0.10
Bs	-0.09	0.07	-0.13	-0.09	-0.01	0.00
ds	0.20	0.22	0.22	0.22	0.18	0.19
ST_AR	-0.05	-0.07	-0.04	-0.05	-0.08	-0.05
SL_AR	0.31	0.17	0.37	0.33	0.28	0.23
MT_AR	0.01	0.00	0.01	0.01	0.01	0.00
HP_width	0.48	0.43	0.45	0.46	0.43	0.49
htc_ag	-0.15	-0.13	-0.16	-0.15	-0.17	-0.14
htc_WJ	0.09	0.09	0.09	0.09	0.09	0.09
Pd_cu	0.38	0.35	0.36	0.37	0.35	0.39
Khp_C	0.00	0.00	0.00	0.00	0.11	-0.03
Khp_R	0.30	0.43	0.31	0.31	0.24	0.32

heat generation and the coolant. The stator aspect ratio ST_AR is the value of the stator's inner diameter divided by the stator's outer diameter. Therefore, higher ST_AR values relate to relatively short slots. Hence, a negative correlation would mean that shallow slots tend to be cooler since there would be a shorter distance for the heat to be extracted through the back iron cooling fluid and the airgap fluid. Naturally, higher values of copper power loss density would tend to have higher temperatures in the slot. Additionally, slot aspect ratio, slot depth and slot width all have a positive correlation with T_O. This is expected as deeper slots are harder to cool as the hotspot is farther away from the cooling fluid in the back iron. Similarly, wider slots also have an increased distance from the centre of the slot to the tooth sides.

The HP width has a relatively strong positive correlation with the temperature difference. This trend was highlighted earlier in Fig. 6(b). The HP radial thermal conductivity has a strong correlation in all HP designs, though it is strongest for the HP B. The thermal conductivity in the tangential direction has a near-zero correlation with temperature difference.

A very interesting correlation is the back iron convective coefficient (htc_wj). The low correlation values clearly suggest that as long as the values are higher than the lower bound of 500 W/m^{2}K, then a higher value of temperature reduction can be achieved. Therefore, to maximise the temperature difference it is critical to find materials with higher thermal conductivity values in the radial direction.

d. Multiple Linear Regression

Multiple Linear Regression (MLR) [27] is used to describe the relationship between the input parameters and the output response. The MLR is a statistical technique that uses several explanatory variables to predict the outcome of a response variable. The same input variables introduced in the correlation analysis are used for this purpose.

The results are summarised in Tables A1 and A2 in the Appendix, wherein the last row is dedicated to the overall regression of the responses observed. Percentage values are listed, therefore the regression expressed was 79.68% for the T_O response where 100% means that the regression model perfectly describes the responses. Indeed, the regressions identified in this study are no more than 80%, since this problem is not linear in nature, and the proposed search space has been deliberately very widely distributed.

Yet, values higher than 60% and 70% of linear model regression are acceptable values [27],[28]. Thus, having an average regression for the seven models of 79.51% is promising.

The coefficients of the regression equations are also listed in Tables A1 and A2 in the Appendix. An example of how to construct the regression equation for the peak temperature of the slot is given in (12) for heat path A.

$$T_A = 91.09 - 0.2888\,Slots + 0.11016\,SID - 0.10374\,htc\_ag - 0.007184\,htc\_WJ + 0.32064\,Pd\_cu - 0.00078\,Khp\_C - 0.03768\,Khp\_R - 0.00032\,Lstk - 152.20\,ST\_AR + 3.012\,SL\_AR + 0.061\,MT\_AR - 12.115\,HP\_width + 1.3661\,bs + 0.8213\,ds \quad (12)$$

The model has an average regression of 73.2% for the temperature difference model, which is still higher than 70% and thus in an acceptable range.

Nevertheless, these models are linear, so whilst the regression is acceptable for a linear model, it can be improved. Therefore, a NN model is proposed in the following subsection, which is believed to increase the regression.

e. Neural Network Regression Model

A NN regression model is developed to improve the regression model compared to the MLR approach. As the latter has a high number of independent variables, as well as non-converging result patterns, NNs are proposed to model the system. The same variables are used for the correlation, and linear models are used for the NN model. For the original stator design temperature (T_O), 10 variables are required for the NN model. Nine independent variables are needed to model the temperature, plus the number of slots as an extra dependent variable. For the slot that does not have a HP, the variables related to the HP, such as the width and thermal conductivity, are omitted from the model. The input variables are listed below:

- **Geometric variables**
  - Stator inner radius, stator aspect ratio, slot aspect ratio, motor aspect ratio, HP width (not included in the T_O model), and number of slots.
- **Boundary condition variables**
  - HP thermal conductivity in the radial and circumferential directions (not in the T_O model), heat transfer coefficient at the air gap and the back iron surfaces, and copper power loss density.

The three models developed are:

1) slot temperature without the HP (T_O);
2) temperature of the other 6 HP shapes (T_A: T_F);
3) temperature difference (Td_A: Td_F).

The NN diagram for the first model is shown in Fig. 7(a), with 9 inputs, and 1 output. The NN layout for the other three models can be viewed in Fig. 7(b), where there are 6 outputs, an output for each HP shape.

The regression is equal to 0.9975. The results show that the NN model is very promising in predicting the temperature of different shapes. The regression for the NN model for the peak temperatures for slots with HPs A to F is very effective with a regression of 99.27%. The temperature difference regressions are at 90.3%. These are indeed relativity lower regression values than the temperature model regression, but they are quite high and can be used to predict the performance of the HPs. Thus far the NN regression model is believed to yield a better-fit model than the linear regression model.
The error histogram is shown in Fig. 8. The Y-axis represents the number of instances where an error range has occurred. The X-axis represents the error between the temperature predicted by the model and the data. Also, the NN breaks down the data into three groups, the training group which is the main group that NN is built on, and then the validation and test group where the model is used to predict and compare to the data. The division is 15%, 15% and 70% for the test, validation, and training groups of data

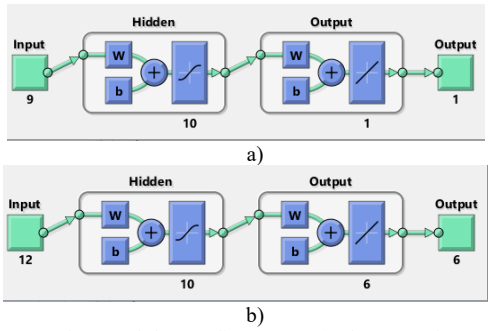

Fig. 7: Neural network layout diagram, a) single output, b) 6 outputs.

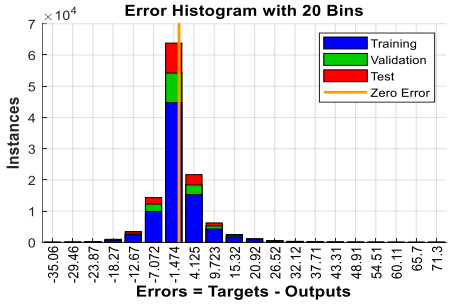

Fig. 8: Neural network residual plot of slot temperature with HP.

V. EXPERIMENTAL SETUP, RESULTS AND MODEL VALIDATION

This section discusses the model validation through thermal FEM and the experimental testing of the HP. The experimental validation is performed on the T-shaped HP, as it exhibited better performance in the majority of the studied cases. Future work should investigate other HP shapes and further optimize HP designs for various applications. Firstly, a description of the built motorettes, and then the testing setup details are provided. Finally, the results from the thermal experiments are presented and analysed.

a. Thermal FEM Model Validation

A thermal FEM model was developed to validate the proposed HP shapes and the LPTN model, as illustrated in Fig. 9. The HP material was assigned a thermal conductivity of 180 W/mK. To ensure a fair comparison, consistent boundary conditions and heat inputs were applied to all shapes. The FEM results demonstrated good agreement with the LPTN model, with a relative accuracy within 5-10%.

The thermal maps in Fig. 9 reveal the effectiveness of all shapes in mitigating hotspot and average slot temperatures. Shapes B and F exhibited the most significant temperature reductions, while shape E showed the least promising results.

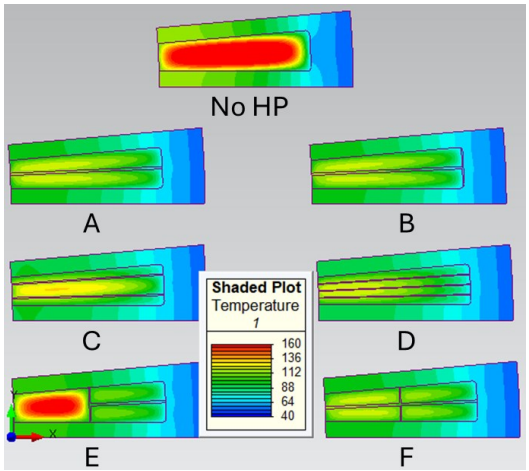

Fig. 9: Thermal FEM model validation of all the HP shapes.

b. Motorettes Description

The first motorette (Moto 1) is the baseline case without an HP, thus representing case T_O. The second motorette presented (Moto 2) has a copper HP built to represent shape 'B'. The HPs are made of back-to-back 'L' shapes which are bonded together to form a 'T' shaped HP. The overall details are depicted in Figs. 10 and 11. The axial stack length is 151 mm. Three concentric coils were connected in series.

In total, there were 32 T-type thermocouples (TC) measurement locations in Moto 1, and 29 for Moto 2 with the HPs installed, and temperatures are recorded through data loggers (Pico Technology TC-08). The motorettes were treated with resin through a Vacuum & Pressure Impregnation (VPI) process.

c. Experiment Setup

The motorettes have three equally sized 6 mm diameter cooling channels, which are located directly under a slot. The motorettes were made from solid non-laminated steel. These design choices were carefully considered to avoid non-uniform contact resistances, leakage and any manufacturing uncertainties that may arise.

The testing setup is shown in Fig. 11. A temperature control unit (Tool Temp, TT-188) is used to maintain a steady cooling fluid temperature of 40 °C. A flow meter (Hydrotechnik, CVC05W3B-A353) was used to monitor the flow rate, which ranged from 2 to 12 litres/min. Also, the temperature at the inlet before the motorettes and at the outlet was measured and recorded.

The motorettes and main pipes were wrapped with a thermally insulating blanket to minimise losses to the environment. Heat was supplied to the coils using a DC power supply connected to the terminals of the windings in power control mode, and the three coils were connected in series, and through a circuit breaker for protection.

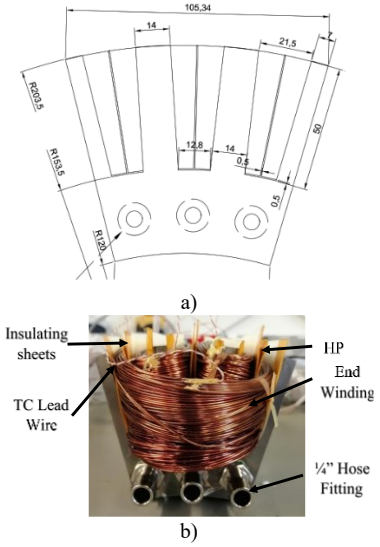

Fig. 10: Motorette a) dimensions and b) windings for Moto1 and Moto2.

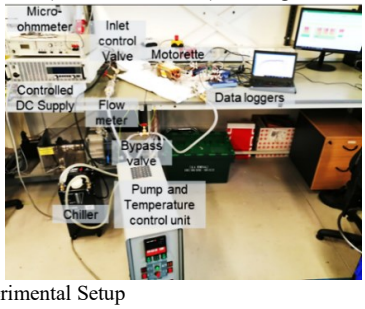

Fig. 11: Experimental Setup

This article has been accepted for publication in IEEE Transactions on Transportation Electrification. This is the author's version which has not been fully edited and content may change prior to final publication. Citation information: DOI 10.1109/TTE.2025.3537161

d. Experimental Results

The experimental results were compared to those of the LPTN model in Fig. 12. For the first motorette a discrepancy range from 0% to 7.8 % was achieved, where the difference tends to increase with higher temperature and power loss ranges. The average difference was less than 3 °C due to the fidelity of the LPTN to represent all material layers appropriately.

The copper B-shaped HP motorette shows a good match between the LPTN and the experimental results. The average absolute and relative errors at a flow rate of 12 litres/min are approximately 3 °C (3% relative error).

Overall, these errors are in an acceptable range for these types of manufacture and thermal tests, considering the difficulty of matching the same boundaries such as the exact flow rate, the convective heat transfer coefficient and perfect thermal insulation.

Therefore, this LPTN gives the confidence to push forward in the research of considering other design variations which will be explored in future publications.

VI. HP ELECTROMAGNETIC LOSSES

A critical aspect that may be overlooked is assessing the inter-dependent effects of the HP and the electromagnetic circuit. In this section, the losses that may be generated in the HP are computed through full-scale transient electromagnetic FE simulation. The losses are assessed at different operating frequencies that translate to a different operating speed for the same motor design. Afterwards, those losses are introduced to the LPTN model to fully evaluate the HP more comprehensively, by considering the net cooling benefit for each HP between self-heat generation and its cooling capacity.

a. HP Loss Quantification

The copper sheet electrical conductivity is set to 5.77e7 Siemens/m. The losses generated in these sheets are quantified through a full-machine electromagnetic FE transient simulation. The frequencies explored range from 21 Hz to 672 Hz and at five different current loading values from 48 to 83 A_{peak}, thus, corresponding to the power losses tested in the experimental setup from 100 to 300 W. The ratio between the winding losses and the losses generated in the HP sheets are quantified and plotted in Fig. 13, and the evaluation of the winding temperatures with these added losses is illustrated in Fig. 14.

The losses generated in the copper-based HP for the motorette 2 design are plotted in Fig. 13. It is evident that these losses reach quite substantial values even at very low frequencies, for example, at 21 Hz it reaches a quarter of the winding losses, and at 672 Hz is reaches 25 times the winding losses. Therefore, loss mitigation should be taken into account when designing these HPs, such as HP segmenting or slicing to prevent high eddy current losses. However, the above results and observations do not compromise the main outcomes of the paper, while they suggest further understating and improvements in the passive slot HP concept.

b. Accounting for the HP Losses

The eddy current losses quantified are used in the LPTN model to evaluate the use of a specific HP material in a motor. The performance of the copper HP was very promising in terms of temperature reduction for the same winding loss

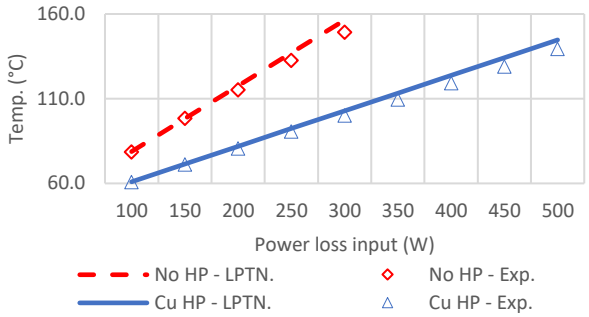

Fig. 12: LPTN vs experimental results for Copper HP shape B .

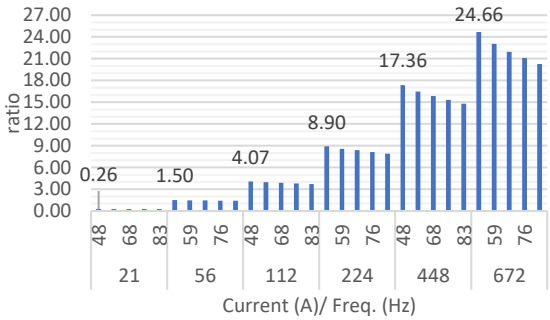

Fig. 13: Ratio of HP losses to winding losses of copper HP.

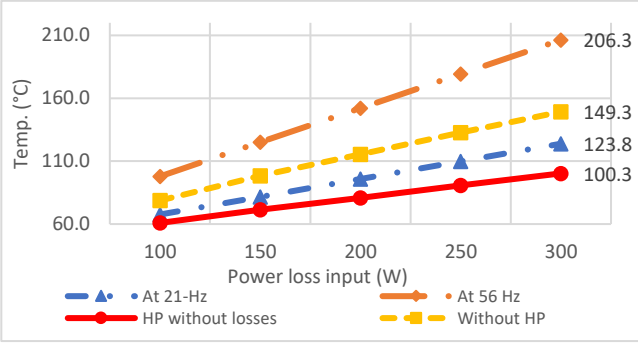

Fig. 14: Average temperatures with HP losses of Copper.

input as discussed earlier. Indeed, it can result in a temperature difference of up to 60 °C. However, it also produces losses equal to a quarter of the winding losses at frequencies as low as 21 Hz. As depicted in Fig 14, the copper-based HP is only acceptable for operating at very low frequencies sub 20 Hz – which limits its practical implementation at high frequencies without significant modification of the HP. These modifications are out of the scope of this paper. Furthermore, the performance of the same motorette without the HP losses is plotted as reference lines for comparison. However, it still can be viable for large generators, such as those found in wind turbines, when operating at low rotational speeds or generally speaking low electrical frequency machines. Therefore, exploring other substitute materials that can be feasible at higher frequencies is critical and will be addressed in future works.

VII. CONCLUSION

This paper explored the whole concept of in-slot thermally conductive HPs in an extensive and detailed manner. The novelty in this paper is the generalised LPTN model which has been proposed to represent six feasible conductive HPs for the heat to be dissipated throughout and out from the slot. Whilst HPs have been proposed before, the range of shapes, and the in-depth analyses of the HP performance for a very large range of geometric, thermal and electromagnetic boundary condition parameters present behaviours that significantly expand the understanding of in-slot HPs. The

experimental validation testing of the fluid and thermal modelling provided rigorous and convincing comparative results (within 3%) to show the model's reliability.

The multivariant and extensive search space of various shapes and sizes of motors and slots can be used as a library and reference for future researchers and designers for the application of HP in electrical machines. The HP can indeed reduce the slot hotspot temperature by a promising large margin of up to 60-100 °C, especially for high power-density applications.

It is recommended to consider materials with as high as possible thermal conductivity across the thickness and very low electrical conductivity. Thus, thermal conductivities higher than 100 W/mK are recommended and thicknesses that are higher than 0.5 mm and more are encouraged. Hence, this paper has analysed in an elaborate manner the performance of the HP for a generic pool of HP materials, shapes and motor design.

The paper also presented a unique in-depth analysis of the HP performance considering the large pool of data and drew a general conclusion using the correlation analysis. Additionally, a linear multivariant regression model is presented, as well as an Artificial Neural Network as a tool for predicting other shapes and operating conditions. The paper concludes with an analysis of the electromagnetic losses that are generated within the HP and how they may affect the thermal performance of the HP.

Future work will explore using different materials experimentally and discuss the design of an aircraft propulsion motor from the electromagnetic and thermal perspectives, where the implementation of an HP, using the outcomes from this paper, will also be explored as an enhancement to the thermal management and holistic machine performance characteristics.

APPENDIX

TABLE A1
TEMPERATURE'S REGRESSION EQUATION COEFFICIENTS.

	T_O	T_A	T_B	T_C	T_D	T_E	T_F
Constant	69.49	91.09	94.60	91.99	94.70	83.22	91.97
Slots	-0.349	-0.289	-0.250	-0.295	-0.277	-0.314	-0.277
SID	0.130	0.110	0.099	0.111	0.107	0.123	0.108
htc_ag	-0.155	-0.104	-0.087	-0.103	-0.095	-0.130	-0.104
htc_WJ	-0.006	-0.007	-0.008	-0.007	-0.007	-0.007	-0.007
Pd_cu	0.388	0.321	0.292	0.324	0.310	0.359	0.316
Khp_C	-0.001	-0.001	-0.001	-0.001	-0.001	-0.007	0.002
Khp_R	-0.002	-0.038	-0.075	-0.039	-0.045	-0.014	-0.041
Lstk	0.000	0.000	0.000	0.000	0.000	-0.001	0.000
ST_AR	-178.8	-152.2	-134.7	-153.4	-148.3	-170.1	-151.0
SL_AR	6.327	3.012	2.772	2.855	2.476	4.275	2.911
MT_AR	0.208	0.061	0.049	0.052	0.046	0.159	0.072
HP_width	0.809	-12.11	-14.75	-11.42	-13.52	-4.34	-12.7
bs	1.518	1.366	1.202	1.411	1.364	1.336	1.256
ds	0.819	0.821	0.807	0.809	0.808	0.856	0.849
Regression%	***79.68***	***79.47***	***79.56***	***79.41***	***79.38***	***79.51***	***79.51***

TABLE A2
TEMPERATURE'S DIFFERENCE REGRESSION EQUATION COEFFICIENTS.

	$Td_A = T_O-T_A$	$Td_B = T_O-T_B$	$Td_C = T_O-T_C$	$Td_D = T_O-T_D$	$Td_E = T_O-T_E$	$Td_F = T_O-T_F$
Constant	-21.60	-25.11	-22.50	-25.21	-13.73	-22.480
Slots	-0.060	-0.099	-0.054	-0.072	-0.035	-0.072
SID	0.020	0.032	0.019	0.024	0.008	0.023
htc_ag	-0.051	-0.068	-0.052	-0.060	-0.025	-0.051
htc_WJ	0.001	0.001	0.001	0.001	0.000	0.001
Pd_cu	0.067	0.096	0.064	0.077	0.028	0.072
Khp_C	-0.001	0.000	-0.001	-0.001	0.006	-0.004
Khp_R	0.036	0.073	0.037	0.043	0.012	0.039
Lstk	0.000	0.000	0.000	0.000	0.000	0.000
ST_AR	-26.58	-44.04	-25.40	-30.49	-8.66	-27.74
SL_AR	3.315	3.555	3.472	3.851	2.052	3.416
MT_AR	0.147	0.159	0.156	0.162	0.049	0.135
HP_width	12.925	15.563	12.234	14.334	5.153	13.518
bs	0.152	0.316	0.108	0.154	0.182	0.263
ds	-0.002	0.013	0.010	0.012	-0.037	-0.029
Regression%	***75.02***	***74.21***	***74.35***	***74.63***	***65.96***	***74.86***

REFERENCE

[1] F. Zhang *et al.*, "Back-Iron Extension Thermal Benefits for Electrical Machines with Concentrated Windings," *IEEE Transactions on Industrial Electronics*, vol. 67, no. 3, pp. 1728–1738, 2020, doi: 10.1109/TIE.2019.2903758.

[2] A. Hebala, S. Nuzzo, P. H. Connor, P. Giangrande, C. Gerada, and M. Galea, "PM Halbach Arrays in Motors: Loss Reduction and Performance Improvements," *23rd International Conference on Electrical Machines and Systems, ICEMS 2020*, pp. 710–715, 2020, doi: 10.23919/ICEMS50442.2020.9291234.

[3] G. J. Atkinson, B. C. Mecrow, A. G. Jack, D. J. Atkinson, P. Sangha, and M. Benarous, "The analysis of losses in high-power fault-tolerant machines for aerospace applications," *IEEE Trans Ind Appl*, vol. 42, no. 5, pp. 1162–1170, 2006, doi: 10.1109/TIA.2006.880869.

[4] R. Aziz, G. J. Atkinson, and S. Salimin, "Thermal modelling for permanent magnet synchronous machine (PMSM)," *International Journal of Power Electronics and Drive Systems*, vol. 8, no. 4, pp. 1903–1912, 2017, doi: 10.11591/ijpeds.v8i4.pp1903-1912.

[5] A. Boglietti, A. Cavagnino, D. Staton, M. Shanel, M. Mueller, and C. Mejuto, "Evolution and modern approaches for thermal analysis of electrical machines," *IEEE Transactions on Industrial Electronics*, vol. 56, no. 3, pp. 871–882, 2009, doi: 10.1109/TIE.2008.2011622.

[6] G. M. Gilson, T. Raminosoa, S. J. Pickering, C. Gerada, and D. B. Hann, "A combined electromagnetic and thermal optimisation of an aerospace electric motor," *19th International Conference on Electrical Machines, ICEM 2010*, pp. 1–7, 2010, doi: 10.1109/ICELMACH.2010.5607893.

[7] D. G. Dorrell, M. F. Hsieh, M. Popescu, L. Evans, D. A. Staton, and V. Grout, "A review of the design issues and techniques for radial-flux brushless surface and internal rare-earth permanent-magnet motors," *IEEE Transactions on Industrial Electronics*, vol. 58, no. 9, pp. 3741–3757, 2011, doi: 10.1109/TIE.2010.2089940.

[8] T. Hong, M. Rakotovao, M. Henner, S. Moreau, and J. Savage, "Thermal analysis of electric motors in engine cooling fan systems," *SAE Technical Papers*, no. July, 2001, doi: 10.4271/2001-01-1017.

[9] A. J. Bourgault, P. Roy, E. Ghosh, and N. C. Kar, "A Survey of Different Cooling Methods for Traction Motor Application," *2019 IEEE Canadian Conference of Electrical and Computer Engineering, CCECE 2019*, no. 3, pp. 1–4, 2019, doi: 10.1109/CCECE.2019.8861611.

[10] M. Galea, C. Gerada, T. Raminosoa, and P. Wheeler, "A thermal improvement technique for the phase windings of electrical machines," *IEEE Trans Ind Appl*, vol. 48, no. 1, pp. 79–87, 2012, doi: 10.1109/TIA.2011.2175470.

[11] Y. Yang *et al.*, "Thermal management of electric machines," *IET Electrical Systems in Transportation*, vol. 7, no. 2, pp. 104–116, 2017, doi: 10.1049/iet-est.2015.0050.

[12] A. Trentin *et al.*, "Research and Realization of High-Power Medium-Voltage Active Rectifier Concepts for Future Hybrid-Electric Aircraft Generation," *IEEE Transactions on Industrial Electronics*, vol. 68, no. 12, pp. 11684–11695, 2021, doi: 10.1109/TIE.2020.3040692.

[13] D. Golovanov *et al.*, "4-MW Class High-Power-Density Generator for Future Hybrid-Electric Aircraft," *IEEE Transactions on Transportation Electrification*, vol. 7, no. 4, pp. 2952–2964, 2021, doi: 10.1109/TTE.2021.3068928.

[14] L. John, S. Reuter, D. Becker, H.-C. Möhring, R. Eisseler, and M. Doppelbauer, "Prototype fabrication of complex cooling channels by potting, additively manufactured inserts in an electric motor," in *2023 13th International Electric Drives Production Conference (EDPC)*, Nov. 2023, pp. 1–6. doi: 10.1109/EDPC60603.2023.10372147.

[15] Z. Yao, R. K. Mandel, and F. P. McCluskey, "In-slot Cooling for High Power Density Electric Motor with Encapsulation Channels," in *2022 21st IEEE Intersociety Conference on Thermal and Thermomechanical Phenomena in Electronic Systems (iTherm)*, May 2022, pp. 1–6. doi: 10.1109/iTherm54085.2022.9899559.

[16] Z. Xu *et al.*, "A semi-flooded cooling for a high speed machine: Concept, design and practice of an oil sleeve," *Proceedings IECON 2017 - 43rd Annual Conference of the IEEE Industrial Electronics Society*, vol. 2017-Janua, no. October, pp. 8557–8562, 2017, doi: 10.1109/IECON.2017.8217503.

[17] R. Wang, X. Fan, D. Li, R. Qu, L. Li, and T. Zou, "Convective Heat Transfer Characteristics on End-Winding of Stator Immersed Oil-Cooled Electrical Machines for Aerospace Applications," *IEEE Transactions on Transportation Electrification*, vol. 8, no. 4, pp. 4265–4278, Dec. 2022, doi: 10.1109/TTE.2022.3186800.

[18] Y. Gai *et al.*, "Cooling of automotive traction motors: Schemes, examples, and computation methods," *IEEE Transactions on Industrial Electronics*, vol. 66, no. 3, pp. 1681–1692, 2019, doi: 10.1109/TIE.2018.2835397.

[19] P. Roy *et al.*, "A Comprehensive Review of Thermal Design and Analysis of Traction Motors," *IEEE International Symposium on Industrial Electronics*, vol. 2019-June, pp. 203–208, 2019, doi: 10.1109/ISIE.2019.8781230.

[20] R. Wrobel, P. H. Mellor, M. Popescu, and D. A. Staton, "Power loss analysis in thermal design of permanent magnet machines - A review," *IEEE Trans Ind Appl*, vol. 2015, no. 2, pp. 1359–1368, 2015, doi: 10.1109/TIA.2015.2489599.

[21] K. Bennion, "Electric Motor Thermal Management," *in U.S. Department of Energy Vehicle Technologies Program Annual Merit Review*, 2011.

[22] A. Tüysüz, F. Meyer, M. Steichen, C. Zwyssig, and J. W. Kolar, "Advanced Cooling Methods for High-Speed Electrical Machines," *IEEE Trans Ind Appl*, vol. 53, no. 3, pp. 2077–2087, 2017, doi: 10.1109/TIA.2017.2672921.

[23] A. Hebala, S. Nuzzo, P. H. Connor, C. Gerada, and M. Galea, "Passive In-Slot Heat Path Realisation for Extending the Operating Limits of an Aircraft Propulsion Motor," *IEEE Transactions on Transportation Electrification*, 2024.

[24] S. Wessing and M. López-Ibáñez, "Latin hypercube designs with branching and nested factors for initialization of automatic algorithm configuration," *Evol Comput*, vol. 27, no. 1, pp. 129–145, 2018, doi: 10.1162/evco_a_00241.

[25] "Stephanie Glen. 'Latin Hypercube Sampling: Simple Definition' From StatisticsHowTo.com: Elementary Statistics for the rest of us! https://www.statisticshowto.com/latin-hypercube-sampling/."

[26] P. Arumugam and C. Gerada, "Short term duty electrical machines," *Proceedings - 2016 22nd International Conference on Electrical Machines, ICEM 2016*, pp. 2676–2681, 2016, doi: 10.1109/ICELMACH.2016.7732899.

[27] D. Chicco, M. J. Warrens, and G. Jurman, "The coefficient of determination R-squared is more informative than SMAPE, MAE, MAPE, MSE and RMSE in regression analysis evaluation.," *PeerJ Comput Sci*, vol. 7, p. e623, 2021, doi: 10.7717/peerj-cs.623.

[28] E. Mooi and M. Sarstedt, *A Concise Guide to Market Research: The Process, Data, and Methods Using IBM SPSS Statistic*. 2014. doi: 10.1007/978-3-642-12541-6.

Ahmed Hebala (M'23) received his PhD from the University of Nottingham in 2023, and he received the BSc and MSc degrees in Electrical Engineering from the Arab Academy for Science, Technology and Maritime Transport, Alexandria, Egypt in 2013 and 2017 respectively. In January 2018, he was appointed a Marie Curie Early-Stage Research Fellow and a PhD candidate at the University of Nottingham.

He worked as an assistant lecturer for three years and is currently an Assistant Professor at the Electrical and Control Engineering Department at the AAST.

His main research interests include the design and optimization of electrical machines, thermal management of electrical machines, renewable energy sources, process automation and robotics. He serves as an Associate Editor for the Robotics Integration, Manufacturing and Control (RIMC) Journal.

Peter H. Connor received the M.Eng. and Ph.D. degrees from the Department of Mechanical, Materials and Manufacturing Engineering, University of Nottingham, Nottingham, U.K., in 2009 and 2014, respectively. He is a Senior Research Fellow with the Power Electronics, Machines and Control Research Group, Faculty of Engineering, University of Nottingham.

His research interests are mechanical design and thermal management of electrical machines for industrial power generation and high-speed, high power-density traction, and aerospace applications.

Stefano Nuzzo (M'18) received his PhD degree in Electrical and Electronic Engineering in 2018 from the University of Nottingham, Nottingham, U.K, where he also worked as a Research Fellow within the Power Electronics, Machines and Control (PEMC) Group. He is currently an Assistant Professor in Electrical Machines and Drives at the Department of Engineering "Enzo Ferrari" of the University of Modena and Reggio Emilia, Modena, Italy. His research interests are the analysis, modelling and optimizations of electrical machines intended for power generations, industrial and transport applications.

He is the Secretary of the Electrical Machines, Drives and Automation Committee (TC3) of the IEEE Power Electronics Society (PELS). Also, he serves as Area Editor for the IEEE Transactions on Transportation Electrification and as Associate Editor for the IEEE Transactions on Energy Conversion.

Chris Gerada (M'05-SM'12) received the Ph.D. degree in numerical modelling of electrical machines from The University of Nottingham, Nottingham, U.K., in 2005. He subsequently worked as a Researcher with The University of Nottingham on high-performance electrical drives and on the design and modelling of electromagnetic actuators for aerospace applications. Since 2008, he was appointed as a Lecturer and since 2013, as a Professor at The University of Nottingham. His main research interests include the design and modelling of high-performance electric drives and machines.

Michael Galea (M'13-SM'18, FRAeS) received the Ph.D. degree in electrical machines design in 2013 from the University of Nottingham, Nottingham, U.K. He was promoted to Full Professor of Electrical Machines and Drives with the University of Nottingham in 2019. Since 2021, Prof Galea is with the Department of Electrical Engineering of the University of Malta. His main research interests include design and development of electrical machines and drives (classical and unconventional), reliability and lifetime degradation of electrical machines and the more electric.